A Numerical Analysis on a Solar Chimney with an Integrated Thermal Energy Storage with Phase Change Material in Metal Foam

Bernardo Buonomo*, Lucia* Capasso*, Oronzio* Manca*, Ferdinando* Menale and *Sergio* Nardini

Department of Engineering, University of Campania "Luigi Vanvitelli", Real Casa dell'Annunziata, Via Roma 29, Aversa (CE) 81031, IT

Abstract. In this paper, a two-dimensional numerical investigation on a prototypal solar chimney system integrated with an absorbing capacity wall in a south facade of a building is presented. The capacity wall is composed of a high absorbing plate and an assigned thickness of phase change material in metal foam. The chimney consists of a converging channel with one vertical absorbing wall and the glass plate inclined of 2°. The channel height inside the chimney is equal to 4.0 m, whereas the channel gap is at the inlet equal to 0.34 m and at the outlet it is 0.20 m. The thermal energy storage system is 4.0 m high. The numerical analysis was intended to evaluate the thermal and fluid dynamic behaviors of the solar chimney integrated with a latent thermal energy storage system. The investigation has shown that in all cases PCM has not fully melted during the day and the presence of aluminum foam inside the box attenuates the variation of temperatures during the day. The results show that the three different thickness of the thermal storage system present very similar fluid dynamic and thermal behaviors. For the analyzed configurations, the phase change material does not reach a total melting during the considered day.

1 Introduction

Global warming is one of the main themes of last years. In order to reduce the correlated problems to these climate changes, a lot of technological alternatives was analyzed and promoted such as renewable energies for indoor air conditioning systems. A Latent Heat Thermal Energy Storage System (LHTESS), based on the phase change materials (PCMs), can operate like a passive natural ventilation system if it is combined with a solar chimney. This passive technology can be used during the summer to refresh indoor spaces thanks to the effect of the chimney which pushes the hot air outside, and during the coldest period to warm the indoor space using the daily storage effect of the PCMs [1, 2]. A lot of numerical and experimental studies, conducted over the years, demonstrate the efficiency of using solar energy to solve air conditioning problems. Some studies have demonstrated that the use of solar chimney allows energy savings compared

* Corresponding author: oronzio.manca@unicampania.it

© The Authors, published by EDP Sciences. This is an open access article distributed under the terms of the Creative Commons Attribution License 4.0 (http://creativecommons.org/licenses/by/4.0/).

with air conditioners, especially in hot and humid countries such as Saudi Arabia [3] where more than 70% energy is used for the thermal comfort of civil environments, constantly irradiated by solar energy. Sharma et al. [4] accomplished an experimental study on solar chimney with PCM in box filled with Sodium Sulfate ($Na_2SO_4*10H_2O$) and 15 thermocouples were employed to create temperature maps. The results shown a growing temperature value thanks to the highest thermal performance due to the PCM. Many other experiments were conducted on solar chimney with PCM [5], inside a box with the same height of the chimney [6]. Different number of thermocouples were used in [7, 8] to control the temperature change of the PCM exposed to solar radiation recreated with halogen lamps. This type of lamps was also used in the case of a box with different thickness in [9] or with a fixed thickness of box but in different position respect to the polyurethane inside the chimney in [10]. Zhu et al. [11] used, for an experimental analysis, a box of 30 cm of thickness filled with a mix of paraffin (80%), high-density polyethylene (15%) and graphite (5%). A comparison between the solar chimney behaviors with and without PCM were performed. Some of the previous experiments were also numerically analyzed [12] and the results shown that the initial temperature does not significantly influence the melting time of the PCM. The importance of using the PCM to reduce indoor temperature fluctuations and improve thermal comfort was also demonstrated in [13]. The studies on the PCM incorporated in metal foam show the significant advantages with respect to the PCM storage systems without foam, as indicated for example in [14-16].

In the present investigation, thermal performance of an integrated solar chimney with a latent thermal energy storage (LTES) system was numerically evaluated in transient regime. The LTES was made of PCM embedded in a metal foam and placed in a box behind the vertical adsorbing plate of the solar chimney. The present study seems one of the first investigation on an integrated solar chimney with PCM in metal foam.

The analysis is on a solar chimney system integrated with an absorbing capacity wall in a south facade of a building. The capacity wall is composed of a high absorbing plate and a box with PCM embedded in an aluminum metal foam. The chimney consists of a converging channel with one vertical absorbing wall and a glass plate inclined of 2° from the vertical. The transient analysis is conducted on a two-dimensional model in airflow and the k-ε turbulence model is used. The problem is solved by means of the commercial code Ansys-Fluent. The numerical analysis is intended to evaluate the thermal and fluid dynamic behaviors of the integrated solar chimney. Simulations are made at the June 21, and the results are given in terms of wall temperature distributions, air velocity and temperature fields and transversal profiles.

2 Geometry and mathematical models

The configuration of the analyzed solar chimney is shown in Fig.1. It consists of a channel composed by an absorbing vertical wall of height, L_c, on which is imposed a uniform heat flux, and by a low-emissivity glass wall. The glass is inclined with an angle of 2° respect to the vertical. The width of the inlet and outlet sections of the channel are b_{max} and b_{min}, respectively. The LTES is a rectangular box located on the rear of the absorbing plate. The box has a thickness, s, and the same height of the vertical wall. It is filled with PCM embedded in aluminum foam. The geometrical parameters values are L_c=4.0 m, s=0.0125, 0.025, 0.05 m, b_{max}=0.34 m, b_{min}=0.20 m, α=2°.

To model the solidification and melting of the PCM, the enthalpy-porosity method, given by Voller and Prakash [17], is adopted. In this method, during the melting process, there is no evident separation between the solid zone and the liquid zone but there is a mixed solid-liquid zone defined “mushy zone” and described by the liquid fraction, β:

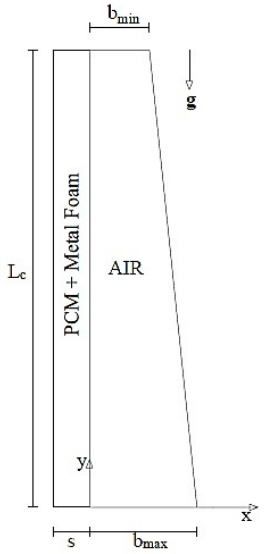

Fig. 1. Solar Chimney sketch.

$$\begin{cases} \beta = 0 & \text{for} \quad T < T_{solidus} \\ \beta = \dfrac{T - T_{solidus}}{T_{liquidus} - T_{solidus}} & \text{for} \quad T_{solidus} < T < T_{liquidus} \\ \beta = 1 & \text{for} \quad T > T_{liquidus} \end{cases} \tag{1}$$

In eq. (1), T is the local temperature, $T_{solidus}$ and $T_{liquidus}$ are the solid and liquid phase temperatures, respectively. The domain is completely solid when $T < T_{solidus}$, while is completely liquid when $T > T_{liquidus}$. The melting occurs when the temperature is included between $T_{liquidus}$ and $T_{solidus}$.

In the present study the Local Thermal Equilibrium (LTE) hypothesis is assumed, the Boussinesq approximation is used to simulate the natural convection of the liquid phase in the PCM and the air in the channel. Moreover, the metal foam is simulated as a porous media, isotropic and homogeneous. Compression work and viscous dissipation are assumed negligibly, and the all thermophysical properties are considered temperature independent except the density. The natural convection of the air flow inside of the solar chimney is considered two-dimensional, unsteady and turbulent and the governing equations are written as follow, for air-zone:

$$\frac{\partial u_i}{\partial x_i} = 0 \tag{2}$$

$$\rho\left(\frac{\partial u_i}{\partial t} + u_j \frac{\partial u_i}{\partial x_j}\right) = -\frac{\partial P}{\partial x_i} + \frac{\partial}{\partial x_j}\left[\mu\left(\frac{\partial u_i}{\partial x_j} + \frac{\partial u_j}{\partial x_i}\right) - \rho\overline{u'_i u'_j}\right] + \rho g_i \gamma\left(T - T_0\right) \tag{3}$$

$$\rho c_p\left(\frac{\partial T}{\partial t} + u_i \frac{\partial T}{\partial x_i}\right) = \frac{\partial}{\partial x_i}\left[\lambda \frac{\partial T}{\partial x_i} - \rho c_p \overline{u'_i T'}\right] \tag{4}$$

With τ the viscous stress tensor; u_i, T, P the velocity components in the directions x_i, temperature and pressure respectively. The turbulent Reynolds stresses $\left(\rho\overline{u'_i u'_j}\right)$ in momentum eq.(3), and the turbulent heat transfer $\left(\rho\overline{u'_i T'}\right)$ in energy eq.(4) are evaluated by an turbulence-model. A k-ε model [18-20], is considered in this work.

The governing equations for the PCM are written in two-dimensional, unsteady and laminar PCM-zone:

$$\frac{\partial u_i}{\partial x_i} = 0 \tag{5}$$

$$\frac{\rho_p}{\varepsilon}\left(\frac{\partial u_i}{\partial t} + \frac{u_j}{\varepsilon}\frac{\partial u_i}{\partial x_j}\right) = -\frac{\partial p}{\partial x_i} + \frac{\mu_p}{\varepsilon}\left(\frac{\partial^2 u_i}{\partial x_i^2} + \frac{\partial^2 u_i}{\partial x_j^2}\right) + S_{xi} \tag{6}$$

Where ρ_p is the density of the PCM and it depends on temperature assuming the Boussinesq approximation, μ_p is the viscosity of the liquid PCM, p is the pressure and vector S_{xi} is the source term defined as [21]:

$$S_{xi} = -\frac{(1-\beta)^2}{\left(\beta^3 - 0.001\right)^3} A_{mush} u_i - \frac{\mu_p}{K} u_i - \frac{C_F}{\sqrt{K}} \rho_p u_i \sqrt{u_i^2 + u_j^2} + \rho_p g_i \gamma \left(T - T_0\right) \tag{7}$$

The first term in eq. (7) simulates the presence of the solid part in the mixed zone, and it is associated to the enthalpy-porosity method, the quantity 0.001 is assigned to avoid zero to the denominator when β, the liquid fraction, tends to zero. A_{mush} is the mushy zone constant, it represents the velocity damping to zero in the solidification process [22,23] and its value is set to 10^5 kg/(m^{3}s). The constant A_{mush} does not affect the behavior of the melting when there is a metal foam in the system as showed by Buonomo et al. [24]. The last term takes into account the buoyancy effect, where T_0 is the reference temperature and γ represents the thermal expansion coefficient. The K and C_F are the permeability and inertial drag factor of the metal foam, respectively.

The energy equation, with the hypothesis of local thermal equilibrium, is:

$$\left(\rho c\right)_{eff}\left(\frac{\partial T}{\partial t} + u_i \frac{\partial T}{\partial x_i}\right) = k_{eff}\left(\frac{\partial^2 T}{\partial x_i^2}\right) - \varepsilon \rho_p H_L \frac{\partial \beta}{\partial t} \tag{8}$$

H_L is the latent heat of the PCM, and t is the time. $(\rho c)_{eff}$ is a weighted average value and it is equal to $(1-\varepsilon)\rho_{mf} c_{mf} + \varepsilon\rho_p c_p$, where ρ_{mf} and c_{mf} represent the metal foam density and specific heat, ε is the metal foam porosity. The density and specific heat of PCM are indicated by ρ_p and c_p. The effective thermal conductivity k_{eff} is evaluated as $(1-\varepsilon)k_{mf} + \varepsilon k_p$ with k_{mf} and k_p the metal foam and PCM thermal conductivities, respectively.

The variation of enthalpy, for unit of volume, in the PCM is evaluated as:

$$\Delta h_{pcm} = \rho_{pcm} h_L \beta + \rho_{pcm} c_v (T - T_0) \tag{9}$$

in which T_0 represents the ambient temperature and it is equal to 294 K.

The PCM chosen for this work is the paraffin wax R56-58 (produced by Merk Millipore) and the thermal properties are listed in Table 1 [25,26]. In the same table are reported also the properties of the aluminum foam [27]. It was chosen aluminum for foam because of its low cost, lower density and weight in relation to other materials.

Velocity and temperature are assumed equal to zero and 294 K respectively, everywhere, as initial conditions. The boundary conditions considered are: at the inlet section, assigned temperature and pressure; at the outlet section, assigned external pressure and external temperature if the velocity is negative and adiabatic condition if the velocity is positive. On the solid walls of the channel the no-slip condition is applied and on the absorbing wall the local solar radiation, as function of time, is multiplied to the transmission coefficient whereas the inclined glass surface is considered adiabatic. In the box with LTES, on the walls the no-slip and the adiabatic conditions are assumed except for the wall adjacent to the channel where heat flux and temperature continuity is supposed.

3 Numerical model

The governing equations (2-4;5,6;8) are solved by means the finite volume method adopting Ansys Fluent code [28]. The Semi-Implicit Method for Pressure-Linked Equations (SIMPLE) is settled to couple pressure and velocity. For unsteady energy and momentum equations the second-order upwind scheme is chosen for discretization of convective terms. The Surface-to-Surface (S2S) model is chosen as radiation model for the open channel with inside the air. In fact, it considers the fluid non-participant to the radiative heat exchange. The grey-diffuse model is used in Ansys Fluent. Since the medium that separates the vertical wall and the glass does not influence the exchange of radiative energy between them, the uniform heat generation, that is transmitted on the aluminum plate, is τE, where τ (equal to 0.68) is the transmittance coefficient of the glass and E (settled with a User Define Function) is the Radiant Energy [29]. The inclined wall is a low-emissivity glass (0.84 external emissivity, 0.04 internal emissivity), it has a coating to reduce heat loss so the solar radiation can enter in the structure and the radiation from the inner surfaces cannot exit. The choice of mesh is a compromise between the quality of the solution and the calculation time, for this reason a sensitivity analysis of the mesh was carried out by analyzing three computational domains, considering only the chimney without the box filled with PCM, Table 2. Taking the mesh n.3 as reference, an evaluation of percentage error ($e_{h\%}$) with respect to this value is made and given in Table 3.

Table 1. Properties of the paraffin wax R56-58 and aluminum foam

Properties	Paraffin	Aluminum foam
Specific heat, C_p (J/kg K)	2100	2719
Density, ρ (kg/m^3)	840	871
Thermal conductivity, λ (W/m K)	0.2	202.4
Viscosity, μ (kg/m s)	0.003	
Thermal expansion, γ (1/K)	0.0004	
Latent heat, H_L (kJ/kg)	120.7	
Solidus temperature, $T_{solidus}$ (K)	323.75	
Liquidus temperature, $T_{liquidus}$ (K)	339.65	

Table 2. Total number of cells per mesh

Mesh	Nx	Ny	Total Cells
1	31	240	7440
2	62	480	29760
3	124	960	119040

$$e_{h\%} = \frac{\left|h_x - h\right|}{h} \tag{10}$$

In equation (10) h is the reference value and h_x is the value whose error is unknown.

At the end of the sensitivity analysis, the chosen grid is the mesh n.2 because it represents the optimal compromise between the accuracy of the simulation and the computational time.

Table 3. Average values and percentage error (eh%) with respect to mesh.

Mesh	T_{wall} [K]	$T_{central\ line}$ [K]	h [W/m^2 K]	Mass flow [kg/s]
1	348.5	298.3	8.89	0.197
2	340.0	302.2	9.84	0.290
3	338.2	302.2	10.0	0.289
Mesh	$e_{h\%}$			
1	3.05	1.29	11.1	31.83
2	0.53	0	1.6	0.35

4 Results and discussion

The numerically examined configuration is a solar chimney realized with a vertical aluminum wall, on which is imposed a heat flux in transient regime, and with an inclined glass wall. Behind the aluminum wall is located a phase change material embedded in an aluminum foam. The heated wall is oriented towards south and simulations are performed considering the structure located in Aversa (Italy) during the June 21 by the sunrise to the sunset.

Figure 2 reports the average temperature profiles, in Fig. 2a, and liquid fractions, in Fig. 2b, inside the box for three different thicknesses of the LTES. Average temperature profiles, reported in the Fig.2a, show similar trend as a function of time. The maximum values of average temperature inside the box is 325 K, 327 K and 328 K for thickness equal to 5 cm, 2.5 cm and 1.25 cm, respectively. In all analyzed cases the complete melting of the paraffin-wax inside the LTES is never attained as noted in Fig.2b, because, the liquid fraction, β, is never equal to 1. The maximum average values of β reached for the three configurations, are equal to 24% for s = 5cm, 36% for s = 2.5cm and 42% for s = 1.25cm.

As shown in Fig. 3a, there is a substantial different between the three configurations in terms of enthalpy variations. In fact, the box with s = 5 cm has as a maximum enthalpy value equal to 1.7x10^7 J/m^3, for s = 2.5cm has a maximum value of 9.8x10^6 J/m^3 while it is almost equal to 5.6x10^6 J/m^3 for s = 1.25cm. The mass flow rate, depicted in Fig.3b, shows a very similar trend as a function of time for the three considered configurations. There is a constant value almost equal to 0.18 kg/s for about 3 hours, from 10:30 to 13:30 (2.0x10^4 s-3.0x10^4 s).

In Fig.4 are reported the velocity profiles, as a function of time, for the three analyzed configurations. At inlet section, in Fig. 4a, for *s*=1.25 cm the maximum velocity is equal to 0.44 m/s, for *s*=2.5 cm it is equal to 0.43 m/s and it is equal to 0.40 m/s for the LTES with thickness of 5 cm. At outlet section, in Fig.4b, the maximum values of velocity are equal to 0.74 m/s for the box with *s*=1.25 cm, to 0.70 m/s for the box with *s*=2.5 cm and to 0.62 m/s for *s*=5 cm.

For a better understanding of the solar chimney behavior with LTES filled with PCM in metal foam, a comparison with the integrated system with PCM not embedded in the metal foam [29] is shown in Fig.5. The comparison between the variation of enthalpy, Fig 5a, and the average temperature of the box, Fig. 5b, are reported. In Fig.5a, it is possible to note that the trend of the enthalpy is similar for the analyzed boxes with and without the metal foam (MF). In the less thick LTES the highest difference is reached at about 2.0×10^4 s. For

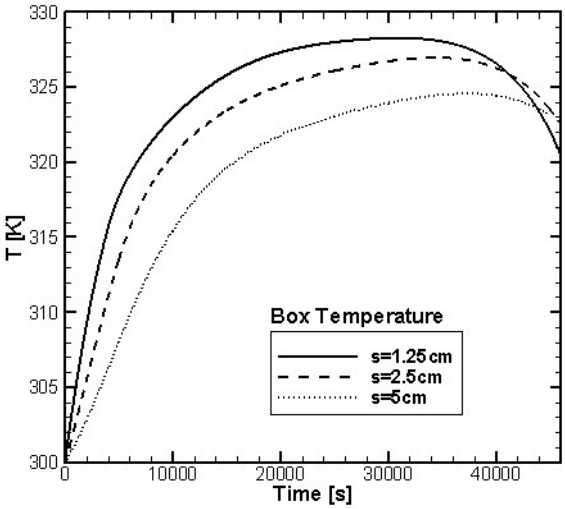

(a)

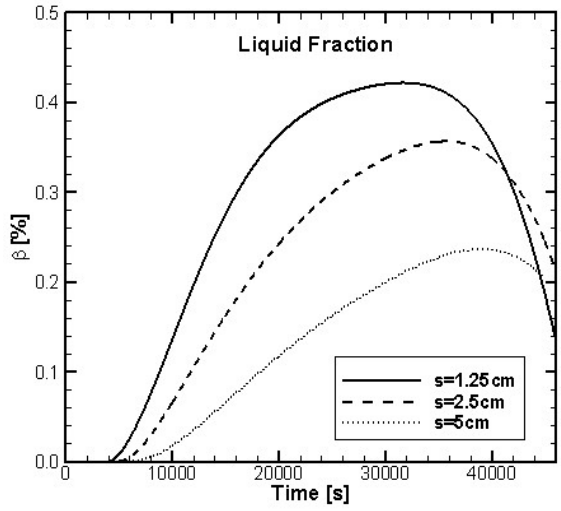

(b)

Fig. 2. (a) Average temperature and (b) liquid fraction profiles as a function of time for different values of PCM thickness

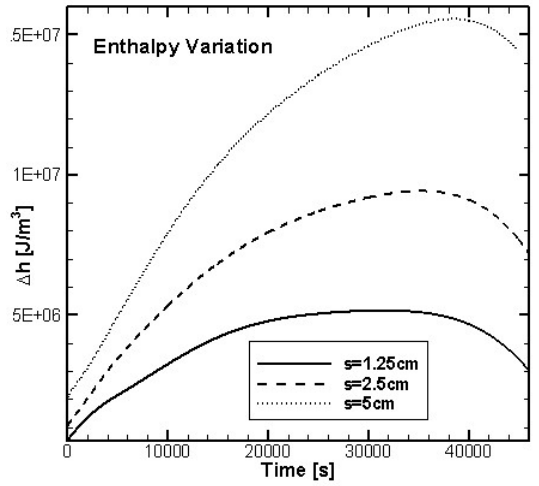

(a)

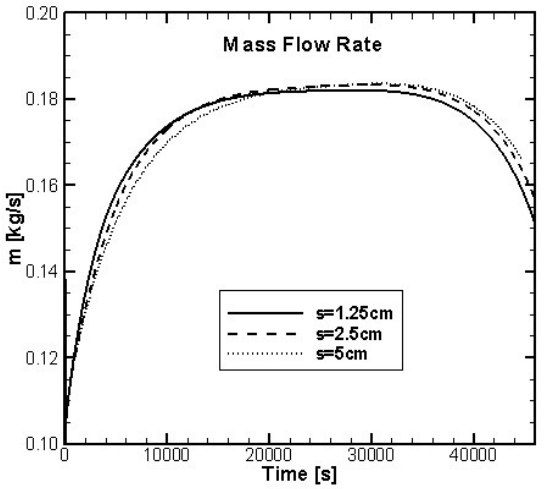

(b)

Fig. 3. (a) PCM enthalpy and (b) air mass flow (at y=4m) profiles as a function of time for different values of PCM thickness

the LTES with *s*=5 cm the maximum enthalpy is $1.6x10^7$ J/m^3 and $1.7x10^7$ J/m^3 for PCM and PCM+MF, respectively. For *s*=2.5 cm the enthalpy variations are equal to $9.4x10^6$ J/m^3 and $9.8x10^6$ J/m^3 for only PCM and PCM+MF, respectively. For the box with *s*=1.25 cm, the enthalpy variation is equal to $5.2x10^6$ J/m^3 with PCM and $5.6x10^6$ J/m^3 with PCM+MF. For the box temperature, in Fig.5b, there are no substantial differences. In fact, the values in both cases, with and without metal foam inside the box, are very similar with a temperature difference of almost 2 K. The maximum average temperature reached inside the box of *s*=5 cm is equal to 326 K with PCM and is equal to 325 K with PCM+MF. For the LTES with *s*=2.5 cm the maximum average temperature is about 328 K for the case with only PCM and it is about 327 K for the case with PCM+MF. For *s*=1.25 cm the maximum average temperature is about 330 K for the system with PCM and is about 328 K for the case with PCM+MF. The highest maximum average temperatures are reached in the case with only PCM.

5 Conclusions

In this paper, a numerical investigation on two-dimensional solar chimney system integrated with an absorbing capacity wall in a south facade of a building was presented. Three different thickness of PCM embedded in an aluminum foam were considered. The problem was solved by means of the Ansys-Fluent code. The enthalpy-porosity method in order to model the solidification and melting process was used and local thermal equilibrium model was assumed for the aluminum foam. A comparison with an equal configuration with only PCM inside the LTES was carried out. The results were shown in terms of liquid fraction, temperature and velocity profiles, variation of enthalpy, mass flow rate as a function of time, both for cases with and without metal foam. The analyses were made at the June 21 from the sunrise to the sunset in transient regime. The results showed for the three different thickness of the LTES the fluid and thermal behaviors were very similar.

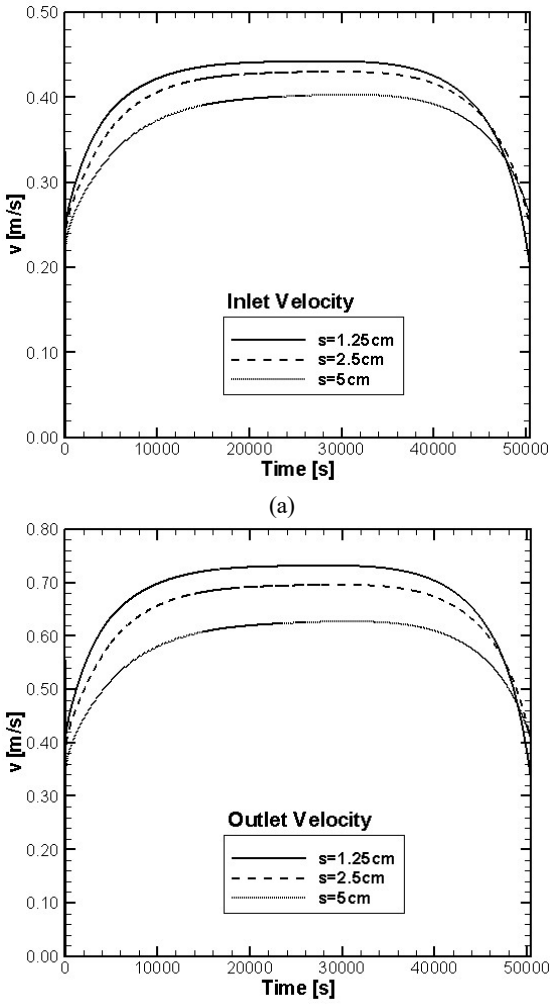

Fig. 4. Velocity profiles as a function of time for different values of PCM thickness: (a) at inlet section (y=0m); (b) at outlet section (y=4m).

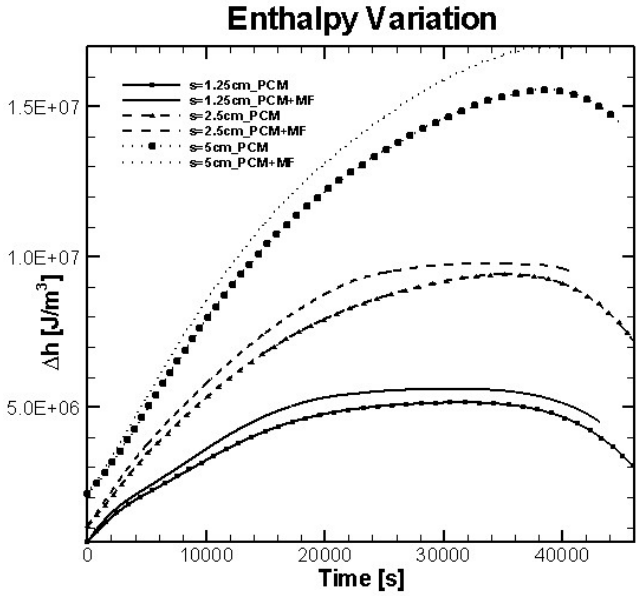

(a)

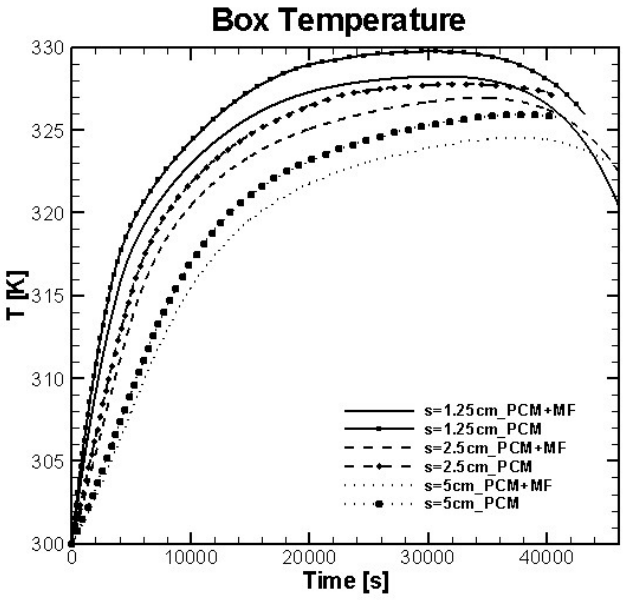

(b)

Fig. 5. Comparison between the profiles inside the LTES: (a) PCM enthalpy, (b) Average temperature

In fact, the maximum average temperatures presented a difference of only 2 K among the three cases. The comparisons among the cases with only PCM and the cases with PCM and metal foam, inside the LTES showed more interesting results. In fact, the presence of aluminum foam inside the box allows to reduce the variation of temperatures during the day. The relevant result concerns the PCM because, in both cases, with and without metal foam, the complete melting inside the LTES was not reached. A value of less than 50% of molten material was detected in all cases with the highest percentage of molten material (β=48%) attained for a box with the thickness of 1.25 cm with only PCM inside of it. The

differences between the liquid fraction and the enthalpy values were evident throughout the loading phase. However slight differences were detected for velocity, air mass flow rate and air temperature inside the solar chimney.

As future development, it could be interesting to analyze the trend of the parameters during the discharge phase and the position of the paraffin wax in a solar chimney inside a box partially filled also to improve the heat transfer and ensure the complete melting of PCM.

6 Nomenclature

A_{mush}	mushy zone costant	(kg $m^{-3}s^{-1}$)
C_P	Specific heat at constant pressure	(J/kg·K)
C_F	inertial drag factor	
D	length of diffusion region	(m)
d_f	ligament diameter	(m)
d_p	pore diameter	(m)
g	gravity acceleration	(m s^{-2})
h	enthalpy for unit of volume	(J/m^3)
H	height of LHTES	(m)
H_L	Latent heat of PCM	(kJ/kg)
K	permeability	(m^2)
Lc	Channel height	(m)
s	Thickness of box filled with PCM	(m)
S	source term	Eqs. (5-6)
t_c	Initial time of convection	(s)
$T_{liquidus}$	Liquidus temperature	(K)
T_o	Ambient temperature	(K)
$T_{solidus}$	Solidus temperature	(K)
T_{wall}	wall temperature	(K)
Greek symbols		
β	Liquid fraction	Eq. (1)
γ	thermal expansion coefficient	(K^{-1})
ε	porosity	
ω	pore size	Pore per Inch (PPI)
κ	Thermal conductivity	(W/m·K)
Subscript		
0	operating	
eff	effective	
i	initial	
m	melting	
mf	metal foam	
p	phase change material	
Δt	time step	

7 Acknowledgments

This research was partially funded by MIUR (Ministero dell'Istruzione, dell'Università e della Ricerca), grant number PRIN-2017F7KZWS and LC thanks the Regione Campania for the PhD fellowship "Impiego dei materiali a cambiamento di fase per il recupero e l'accumulo di energia termica negli edifici sostenibili" in the frame of Dottorati di Ricerca

con Caratterizzazione Industriale, funded with P.O.R. Campania FSE 2014/2020 Asse III – Obiettivo specifico 14 Azione 10.4.5.

References

1. I. Dincer and M. Rosen, *Thermal Energy Storage: System and Application* (2nd ed., John Wiley & Sons, New York, 2010).
2. L. F. Cabeza, *Advances in Thermal Energy Storage Systems: Methods and applications*, (Woodhead Publishing Series in Energy, Sawston, Campbridge, UK, 2014).
3. E. M. A. Mokheimer, M. R. Shakeel and J. Al-Sadah, Energy Build. **153**, 219–230 (2017).
4. S. D. Sharma, H. Kotani, Y. Kaneko, T. Yamanaka and K. Sagara, Int. J. Green Energy **4** (3), 313–324 (2007).
5. Y. Li and S. Liu, Appl. Therm. Eng. **114**, 172–178 (2014).
6. K. E. Amori and S. W. Mohammed, Energy Build. **47**, 450–457 (2012).
7. Y. Li and S. Liu, Energy Build. **80**, 406–414 (2014).
8. Y. Li and Y. Li, Renew. Energy **81**, 338–346 (2015).
9. L. Bin, L. Peng, M. Xiaoyan, S. Jianfei and Y. Zhaodan, Energy Procedia **75**, 521–526 (2015).
10. L. Bin, W. Meixia, W. Qi, M. Shaoli and R. Bennacer, Energy Procedia **139**, 462–467 (2017).
11. N. Zhu, S. Li, P. Hu, F. Lei and R. Deng, Energy **187**, 116057 (2019).
12. Y. Li, S. Liu and J. Lu, Appl. Therm. Eng. **127**, 1119–1131 (2017).
13. C. Jiménez-Xamán, J. Xamán, N. O. Moraga, I. Hernández-Pérez, I. Zavala-Guillén, J. Arce, and M.J. Jiménez, Energy Build. **186**, 384-404 (2019).
14. Y. Tian, and C. Y. Zhao, Energy **36** (9), 5539–5546 (2011).
15. W. Q. Li, Z. G. Qu, Y. L He, and W. Q Tao., Appl. Therm. Eng. **37**, pp 1–9 (2012).
16. P. Zhang, Z. Meng, H. Zhu, Y. Wang, and S. Peng, Energy Procedia **75**, 3091–3097 (2015).
17. V.R. Voller and C. Prakash, *A*, Int. J. Heat Mass Tran. **30**, 1709–1720 (1987).
18. A. Pasupathy, L. Athanasius, R. Velraj and R.V. Seeniraj, Appl. Therm. Eng. **28**, 556 – 565 (2008).
19. B.E. Launder and D.B. Spalding, Comput. Method Appl. M. **3**, 269–289 (1974).
20. A. Ayadi, Z. Driss, A. Bouabidi and M. S. Abid, Energy Build. **139**, 263-276 (2017).
21. A. Ayadi, Z. Driss, A. Bouabidi and M. S. Abid, Ren. Energy **115**, 649-662 (2018).
22. K. Nithyanandam and R. Pitchumani, J. Heat Trans.-T ASME **136**, 051503, (2014).
23. J. Yang, L. Yang, C. Xu, X. Du, Int. J. Heat Mass Transfer **84**, 1008–1018 (2015).
24. B. Buonomo, H. Celik, D. Ercole, O. Manca and M. Mobedi, App. Therm. Eng. **159**, 113980 (2019).
25. J. Yang, X. Du, L. Yang, and Y. Yang, Sol. Energy **98**, 543–552 (2013).
26. X. Hu and X. Gong, Appl. Therm. Eng. **151**, 231 – 239 (2019).
27. V. V. Calmidi and R.I. Mahajian, J. Heat Trans.-T ASME **122**, 557-565 (2000).
28. ANSYS Fluent (Theory Guide).
29. B. Buonomo, L. Capasso, A. Diana, O. Manca and S. Nardini, "A Numerical Analysis on a Solar Chimney with an Integrated Latent Heat Thermal Energy Storage," Proceedings of 74th National Conference ATI, 11–13 September 2019 Modena, Italia.